Canadian Conference - Pacific Conference on Earthquake Engineering 2023
Vancouver, British Columbia
June 25th – June 30th, 2023

Rollout of the Metro Vancouver Network-based Earthquake Early Warning System

Anton Zaicenco [1*], Iain Weir-Jones [2] and Amin Kassam [3]

[1]Senior seismologist, Weir-Jones Engineering Consultants Ltd., Vancouver, BC, Canada
[2] Principal, Weir-Jones Engineering Consultants Ltd., Vancouver, BC, Canada
[3] Division Manager, Shared Utility Services at Metro Vancouver, Vancouver, BC, Canada
[*]anton.zaicenco@weir-jones.com (Corresponding Author)

ABSTRACT

The Metro Vancouver network-based EEW system was designed, built, and commissioned in 2021/2022 as part of the pilot project "EEW and Strategic Response System". The project delivered a robust EEW application, and a Structural Health Monitoring (SHM) service for some of the critical infrastructures operated by Metro Vancouver. Its deliverables are utilized by operations staff within the water system infrastructure. The project builds on two decades of experience of designing, installing, and operating a number of on-site early warning systems protecting various public and private facilities in British Columbia, Washington and Oregon.

Metro Vancouver is the wholesale supplier of safe, clean drinking water to member jurisdictions who in turn distribute the water to the region's 2.8 million residents. Metro Vancouver supplies on average 1.0 billion liters a day through a vast water supply system which includes five dams, two water treatment plants, 27 in-system storage reservoirs and tanks, 19 pump stations, 8 disinfection facilities, and over 520 kilometers of large-diameter transmission water mains. Metro Vancouver is undertaking numerous measures to harden its facilities to withstand seismic events, yet the EEW and SHM initiatives are meant to add to our emergency response capabilities.

The EEW system architecture employs a distributed computing framework. It is designed to use a client-server model where communication between the nodes relies on the Internet. To minimize false positives and corresponding expensive downtime, each station incorporates a robust algorithm for detection and characterization of P waves. To ensure reliable, secure, and fast message passing over the WAN/Internet, a novel communication protocol was developed and implemented. The size of the data packets sent to the server is minimized by pre-computing the vector of the primary seismic event parameters at the client side. These messages are then passed to the server, which aggregates information from all clients and computes the secondary set of the seismic event parameters using the assumption of a point source model.

Soon after the EEWS installation, the network detected and recorded its first earthquake on December 17th, 2021. This was a M3.7 event with an epicentral distance to the closest station of about 50km. Statistical distributions of the event magnitude and the epicenter coordinates were calculated. No alarms were issued since the event parameters were below thresholds determined by design and triggering criteria. The SHM dashboard successfully visualized the post-event structural health information of the target facilities.

Keywords: Earthquake Early Warning, Structural Health Monitoring, Real-time Seismology.

INTRODUCTION

Modern EEW systems attempt to forecast the shaking intensity at a particular site which lies at some distance from the epicenter. Currently, there exists a trade-off between the speed of the warning and the uncertainty in the forecasted seismic intensity – waiting for more data about the earthquake source reduces this uncertainty at the cost of reducing the available warning time. Algorithms based on the point source require first 1-3 seconds of the P wave recorded by inertial seismometers [1]. Real-time high-rate GPS measurements were proposed in order to overcome the magnitude saturation for large events due to instrument limitations, ground tilting, and saturation of frequency/amplitude-magnitude relationships [2].

EEW systems are generally divided into two types: (a) network-based, and (b) on-site. In the network-based approach, the regional network locates the epicenter and calculates the magnitude. The on-site method uses a record of the first few seconds of the P wave and attempts to predict the intensity of the strong ground motion at the same site. In the on-site algorithm, the size of the earthquake is related to the period parameter, τ_c, while the peak initial displacement amplitude, P_d, has a strong correlation with the peak ground velocity PGV [3].

The scaling of magnitude with P wave ground displacement for a large data set of M4.5-9.0 earthquakes recorded by the Japanese K-NET and KiK-net networks was studied by Trugman et al. [4]. It has been demonstrated that this scaling exhibits saturation that depends on the length of the measurement time window, while the true value of P_d is only achieved once the moment rate function peaks. If the rupture duration is less than measurement time window, then there should be a linear scaling between magnitude and $\log_{10}P_d$. The saturation model provides a basis for a rapid probabilistic method for calculating uncertainties in the displacement-based magnitude estimates of the EEW systems.

The US west-coast-wide ShakeAlert EEW system uses an ElarmS network-based algorithm, which relies on a minimum of four stations to alert, but only requires 0.2s sample from these stations [5]. The OnSite algorithm uses a single-station approach and requires a 3s window of the P wave record to detect an earthquake. The ShakeAlert decision module (DM) receives event notifications from both EEW algorithms, which include estimated event location and magnitude, and creates alerts using a weighted average (Böse et al. [6]). ElarmS uses an STA/LTA picker to identify a trigger on the high-pass-filtered vertical component, and an additional H/V<0.95 trigger check to prevent S-wave triggers from coming into the system. Predominant period (τ_p) and peak amplitudes (P_d) are used to estimate the event magnitude.

The FinDer algorithm, proposed by Böse et al. [7], was designed to improve the ShakeAlert system performance during the large-magnitude earthquakes (M>6). FinDer provides estimates of the centroid position, length and strike of the fault rupture based on a rapid near- and far-source classification and comparison with precalculated templates.

To address the shortcomings of the point-source models, Kodera et al. [8] proposed using a propagation of local undamped motion (PLUM) algorithm, a wavefield-based approach that predicts ground motion directly from observed shaking distributions, without estimating source parameters. PLUM uses MMI threshold to trigger an alert using one of several stations. Attenuation (damping) is introduced into the wave propagation to estimate more accurate seismic intensity distribution. However, the PLUM algorithm is optimized for dense seismic networks.

A variation of the on-site algorithm was implemented by Parolai et al. [9]. P_d computed from the first few seconds of the low-passed P wave was used to estimate the PGV of the horizontal components using empirical relationships, and establish a traffic light system for the possible structural damage.

To address the issue of instability associated with the parameter τ_c describing predominant period of the P wave, Simons et al. [10] proposed a wavelet-based technique. The authors demonstrated that scale-dependent threshold amplitudes derived from the wavelet transform of the first few seconds of the P wave are predictive of earthquake magnitude.

The accuracy of EEW systems was explored by Minson et al. [11]. They established that correct alerts are not expected to be the most common EEW outcome even when the earthquake magnitude and location are accurately determined. They emphasized that even an ideal EEW system, with perfect information about the final magnitude and extent of the earthquake rupture and perfect estimates of the median expected ground motion, will produce missed alerts and false alerts because of the ground motion variability incorporated in the Ground Motion Prediction Equations, GMPEs.

In this paper we describe a network-based EEW system, which is augmented by the SHM components. The algorithm uses the assumption of a point source model, employs a novel method for the P wave detection, and blends the methodologies of the on-site and network-based algorithms to locate the earthquake, establish its size, and predict the main parameters of the strong ground shaking. The system employs a sparse seismic network installed on critical facilities in the Metro Vancouver area. It became fully operational in early 2022 providing alerts for the operations staff within water system infrastructure.

OUTLINE OF THE SYSTEM

The Metro Vancouver pilot network-based EEW system consists of 3 stations equipped with multiple inertial seismometers and was designed, built and commissioned in 2021/2022, see Figure 1. The system provides facility operators at each site with customized early warning and relies on the Internet to exchange messages between the nodes and maintain the system remotely. Each station is equipped with one or several multi-channel 24-bit data acquisition systems collecting seismic data at the rate of 2kHz. All units are synchronized with the GPS time and reside on a private LAN to ensure reliable real-time data streaming to the on-site industrial computers. One of these computers acts as a central node, which hosts EEW network-based server application.

Figure 1. Seymour Capilano Filtration Plant, the largest water filtration plant in Canada, is equipped with the EEW and SHM sensors. It is one of 3 GVWD facilities included in the network-based EEW system.

In addition to the EEW application, one of the stations is equipped with the SHM components. They include 3 multi-channels data acquisition units and a set of high dynamic range bi- and tri-axial force-balanced accelerometers monitoring the structural health of the critical facility. Once a seismic event is detected, the system health parameters are updated via the web-based dashboard running on the on-site computer. In addition, system identification can periodically be conducted offline via singular spectrum analysis using the records of low-magnitude events with poor SNR.

The novelty and value of this EEW solution is exemplified by the robust event detection algorithm and distributed computing architecture which eliminates the need to stream all data to the data center in real time. In this way, secure short messages passing between the client and the server occur only when an event is detected, thus reducing the bandwidth requirement, lowering the latencies, and improving the overall system reliability. The following sections outline the EEW algorithm and briefly introduce the SHM methodology. For illustrative purposes the records of a M3.7 earthquake which occurred on December 17th, 2021 have been used.

EEW ALGORITHM

P Wave Detection

P wave detection and classification is the first and one of the most important steps of the EEW algorithm. Robust detection and speed are critical for minimizing false alarms and algorithm efficiency. The P wave event detection is based on the polarization analysis of the symmetric positive definite covariance matrix $\boldsymbol{\Sigma}\in\mathbb{R}^{3\times3}$ of the components of the triaxial inertial seismometer $\mathbf{B}\in\mathbb{R}^{n\times3}$. This analysis requires eigen-decomposition achieved using a QR algorithm, which is performed in real time:

$$\boldsymbol{\Sigma} = \mathrm{cov}(\mathbf{B}) = \mathbf{Q}\boldsymbol{\Lambda}\mathbf{Q}^{-1} \tag{1}$$

Figure 2 shows P wave detection of M3.7 event at each station of the Metro Vancouver EEW system. Polarization analysis produces a function with a sharp peak around the onset of the P wave. In combination with the amplitude and frequency analysis, and the presence of a multi-sensor array at each site, this method creates a robust detector system which is tolerant to the anthropogenic sources of noise typically present at a site. This is particularly important for mission-critical facilities where the cost of downtime is prohibitively high.

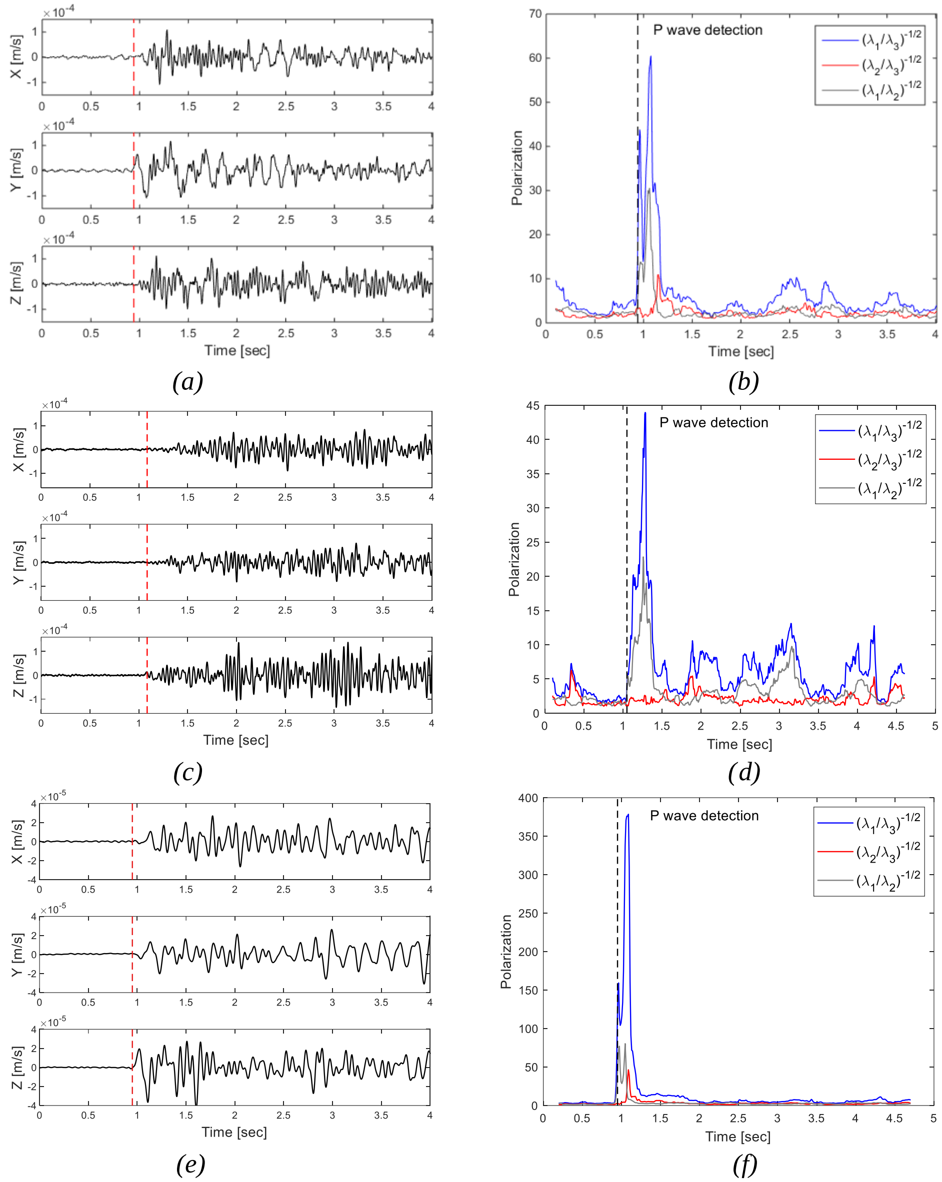

Figure 2. 2021-12-17 M3.7 earthquake: P wave detection via polarization analysis.

This method was first proposed in 2008 by Zaicenco et al. [12] in conjunction with the on-site EEW system installed at the George Massey Tunnel in Metro Vancouver region in 2009 [13]. The method was further developed for the time-frequency domain in [14]. Polarization analysis based on Eq. (3) is applied to any event detected by the STA/LTA pre-trigger continuously running on the on-site computer. The George Massey Tunnel ShakeAlarm system has been in continuous operation for about 14 years [15].

Polarization-based event detection method is not only efficient for identifying P wave arrivals. As well, it acts as a discriminator effectively differentiating between P and S wave components of the ground motion, which is particularly useful in the EEW applications.

Preliminary background noise measurements conducted by the project team at each EEW system location at the beginning of the project demonstrated very low levels of ambient vibration. Analysis of records from the EEW sensors accumulated during the first year of operation confirmed that the background noise is low and normally does not exceed amplitudes greater than 0.00002m/s over a bandwidth of 0-2kHz. The spectral analysis of the records suggested that the ambient vibration at all sites is close to the Peterson High Noise Model, which ensures that the EEW sensors can detect events with magnitude at least M_w=3 at an epicentral distance of ≈100km.

On-site Event Characterization

Since P wave contains information about the slip on the fault plane, our objective is to observe it for as long as possible in order to gain information about the seismic source and its size. At the same time, we want to balance the time of this observation with the need for a quick and useful early warning alert. The kinematic source model based on a circular crack expanding from the center at a constant speed was used by Kanamori [3] to calculate the optimal P wave observation time τ_0=3s. This ensures that for this time, the effective period of the waveform increases with magnitude up to M_w=6.5. For larger events, the circular crack model is less effective. Consequently, a measure of the effective period of the displacement during suggested observation time provides us with an estimate of the size of the event.

It has been established that peak displacement amplitude (P_d) of the P wave correlates well with the expected PGV at the site, and attenuation functions of P_d with hypocentral distance were proposed [1]. Similarly to the effective period, P_d is sensitive to the length of the P wave observation time. Trugman et al. [4] demonstrated that linear scaling between $\log_{10}P_d$ and magnitude is linear when the rupture duration is less than measurement time window, and for τ_0=3s we should be able to effectively resolve magnitudes up to M_w≈6.5.

Consequently, our EEW on-site characterization algorithm adapted the length of the observation time window τ_0=3s and calculated both P_d and the effective period of the truncated P wave to estimate the size of the event and epicentral distance to the site. The algorithm can be summarized as follows: once the onset of the P wave T_i is detected at a station i, the algorithm stores the first few seconds of the P wave recorded by the triaxial inertial seismometer into the vector $\mathbf{d}\in\mathbb{R}^{\mathrm{n}}$. The estimation of the magnitude M_i, and the epicentral distance R_i, for each station are then carried out using this on-site algorithm:

$$M_i = a_1 + a_2 \cdot log_{10}\left(2\,\pi \Big/ \sqrt{\frac{\int_{t1}^{t2} \dot{d}^2(t)dt}{\int_{t1}^{t2} d^2(t)dt}}\right) \tag{2}$$

$$log_{10}(R_i) = a_3 + a_4 \cdot log_{10}(P_d) + a_5 \cdot M_i \tag{3}$$

where the coefficients a_j, j=1,…,5 are computed from the known empirical relationships calibrated with the available regional data. As a result, each station produces a vector of local parameters $\mathbf{p}_i=[M_i\ R_i\ T_i]^{\mathrm{T}}$, these are passed to the server for the final event analysis.

Figure 3 demonstrates results of the on-site event characterization for M3.7 earthquake carried out by three stations. Figures 3(a,c,e) offer a comparison between the amplitude spectrum of the Gabor wavelet analysis with variable number of cycles and evolution of the function $\tau_c(t)$ computed for t_1=1sec and $t_2\in$[1;4]sec (see Eq.(2)). The value $\tau_c(t=4sec)$ agrees well with the peak of the wavelet amplitude spectrum for all stations. Figures 3(b,d,f) demonstrate a good convergence of the estimate of M_i and R_i for all stations, except for the last station, which overestimated R_i due to the local geological conditions near the recording site.

Verification of the Event Characterization Algorithm

As part of the verification process, the adapted event detection and characterization algorithm was used to analyze the event parameters (M and R) of large earthquakes from the Japanese KiK-net database recorded by the NIED strong-motion seismograph network. The dataset of KiK-net seismic records includes 19 large-magnitude events which occurred between 2000 and 2020. The main parameters of the dataset are as follows:

- Magnitude range: 6 – 7.2.
- The epicentral distance range: 10 – 1,000 km.
- The number of records for each event are in the range: 180 – 376.
- The total number of records is 4,899.

Each event k includes a set of triaxial seismic records F_k. The subset of useful records, $U_k \subseteq F_k$, is defined so that it includes a portion of the background noise, followed by the onset of the P waves. Generally, ≈70% of all stations in an event k provided useful records. Most of the records which are not considered useful come from the stations with large epicentral distances (i.e. R>200km), where the peak accelerations are usually small, PGA<0.01m/s^2.

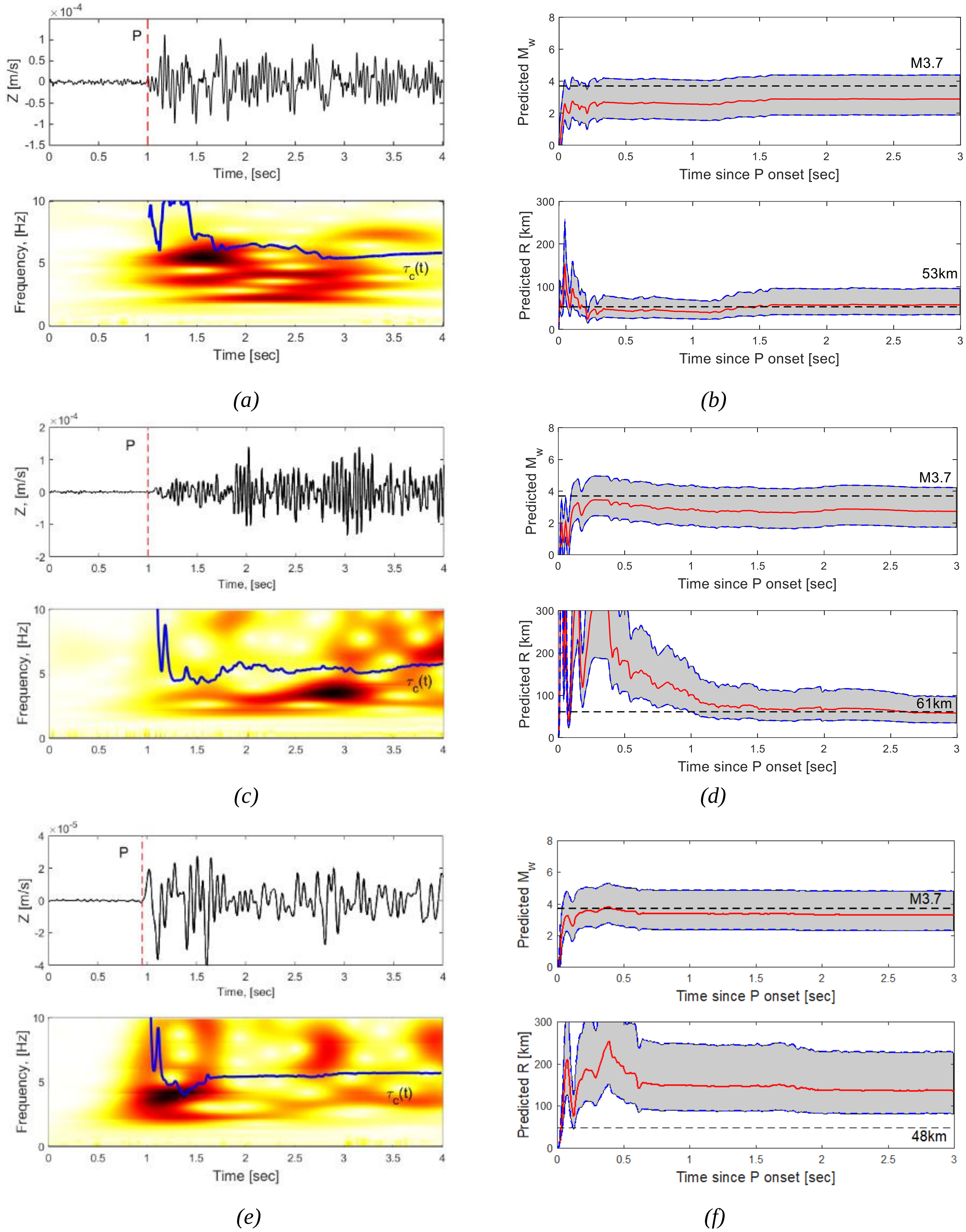

Figure 3. 2021-12-17 M3.7 earthquake record: on-site event characterization using 3 stations: (a,c,e) the detected P wave and corresponding amplitude spectrum of the Gabor wavelet analysis compared with $\tau_c(t)$, (b,d,f) M_i and R_i calculations using Eqs.(2-3). Grey areas indicate the error bounds around mean value shown by red lines. Black dotted line shows the true values of M and R_i.

For each event in the set U_k, the estimates of Weibull distribution parameters for M_k were calculated. It has been established that the modes of the PDFs correlate well with the true value of known event magnitudes.

Figure 4 shows a subset of PDFs obtained during verification studies. These distributions correspond to the events with magnitudes M6.4 (147 records), M6.8 (202 records), M6.3 (106 records), and M7.2 (213 records).

In addition, similar results were obtained from the analysis of records of small-magnitude events collected by the on-site EEW systems in the Metro Vancouver area and Victoria (i.e. George Massy Tunnel, Pattullo Bridge, and the Legislative Assembly of BC systems).

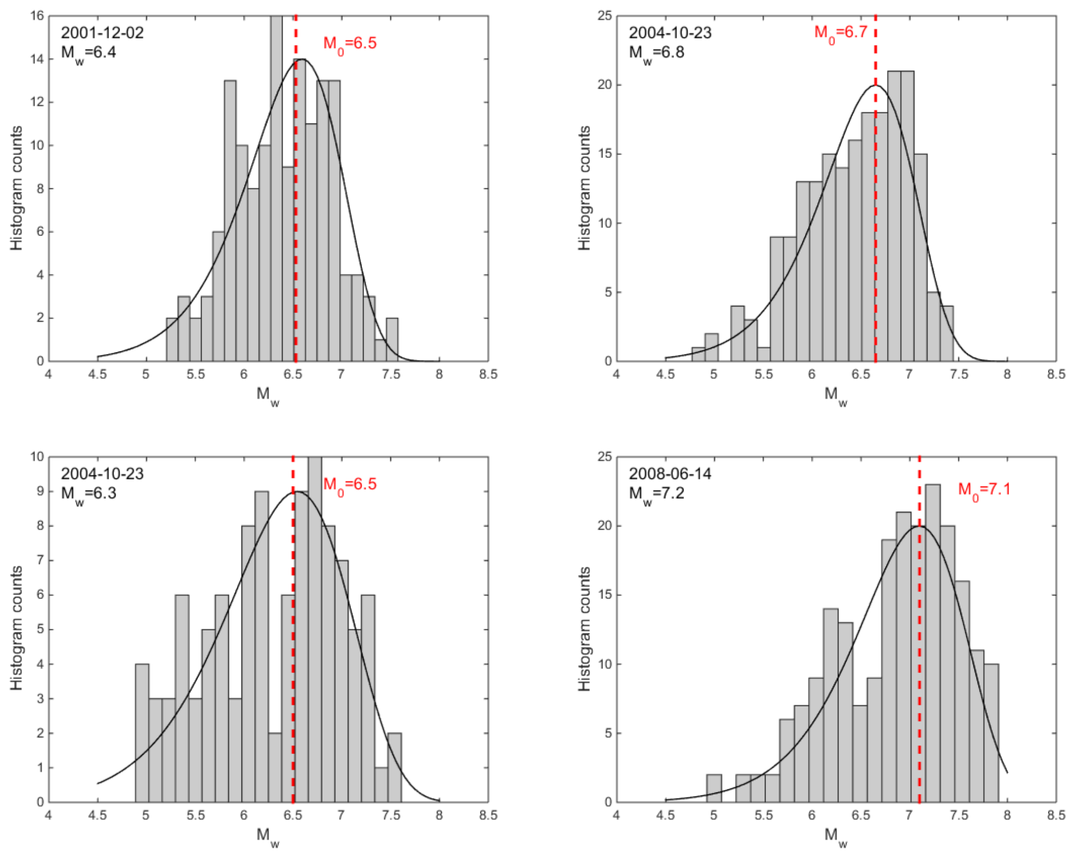

Figure 4. KiK-net strong motion record analysis: histograms of the magnitude calculations from P waves, fitted Weibull distributions f(x;λ,k), and their mode values M_0.

Network-based Event Characterization

Once a seismic event is detected by the inertial seismometers, and the on-site event characterization is completed, the EEW network server receives a vector of parameters $\mathbf{p}_i$ from each station. The arrival times $\mathbf{t}=[T_1\ T_2\ T_3]$ and on-site estimates of R_i are used to locate the epicenter. The task of finding the event coordinates (x_e,y_e) using the arrival times is formulated as a minimization problem for a geometrical domain A in the following way:

$$\text{Minimize } \|\mathbf{t} - \min(\mathbf{t}) - \mathbf{t}_r(x_e, y_e)\|^2, \text{ such that } (x_e,y_e)\in A \tag{4}$$

where $\mathbf{t}_r(x_e,y_e)$ is the vector of the travel times computed for epicental coordinates (x_e,y_e) using the regional velocity model. The estimates R_i are used either as the initial conditions of the minimization problem or as a weighted average component. The non-Gaussian confidence region of the earthquake epicenter located using 3 EEW stations is shown in Figure 5. The confidence region is computed from the chi-squared function arising from the Eq.(4).

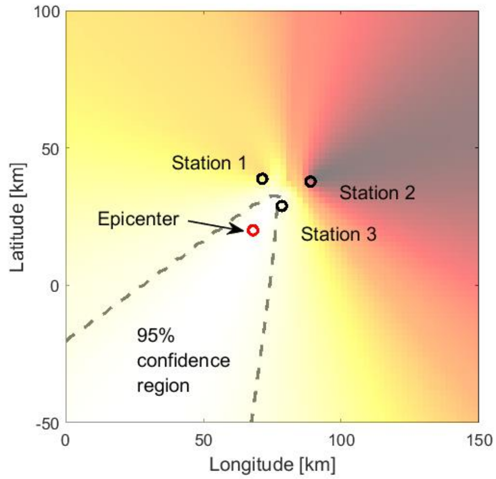

Figure 5. Non-Gaussian confidence region of the located epicenter.

Once the network-based event characterization problem is solved, the estimates of the predicted ground motion parameters at each site are calculated using regional GMPEs. These estimates are used by the local stations to issue an alert.

STRUCTURAL HEALTH MONITORING

The Structural Health Monitoring (SHM) is conducted at one of the sites by means of a set of accelerometers installed on several floors of the R/C structure. The objectives of the SHM were defined set as follows:

- Calculate Katayama Spectral Intensity (KSI), which is based on the integral of the Pseudo-Spectral Velocity response of an SDOF system computed within the limits 0.1 and 2.5 sec.
- Conduct linear response spectra analysis.
- Calculate peak amplitudes (PGA, PGV, PGD), which involves zero-padding, filtering with an 8-pole Butterworth high-pass filter, and integration in the frequency domain.
- Calculate drifts and compare them with thresholds.

In addition, system validations can be conducted periodically using the records of low-magnitude events. For these purposes, the time-domain Singular Spectrum Analysis (SSA) is being employed due to its ability to separate efficiently a signal from its noisy components. The SSA converts a record $\ddot{x}_j$ into a Hankel matrix $\mathbf{H}\in\mathbb{R}^{m\times n}$:

$$\mathbf{H} = \begin{bmatrix} \ddot{x}_1 & \ddot{x}_2 & \cdots & \ddot{x}_m \\ \ddot{x}_2 & \ddot{x}_3 & \cdots & \ddot{x}_{m+1} \\ \vdots & \vdots & \ddots & \vdots \\ \ddot{x}_n & \ddot{x}_{n+1} & \cdots & \ddot{x}_N \end{bmatrix} \tag{5}$$

this implies that an *m*-dimensional vector space spanned by columns formed from the segments of $\ddot{x}_j$ is being formed, while *rank*(**H**)=*dim*(*colsp*(**H**)). A rank-reduced version of **H** is constructed by factorizing it using a singular value decomposition $\mathbf{H}=\mathbf{U\Sigma V}^{\mathrm{T}}$ and retaining only a set of the most important singular values σ_i. Rank-reduced representation $\mathbf{H}_*$ is obtained as follows:

$$\mathbf{H}_* = \mathbf{U}_*\mathbf{\Sigma}_*\mathbf{V}_*^{\mathrm{T}} \tag{6}$$

The filtered signal is reconstructed from $\mathbf{H}_*$ and is a low-rank representation of the original signal $\ddot{x}_j$. Frequency-domain analysis of the filtered signal allows the natural frequencies of the structure to be calculated. As well, it should be possible to recover the state-space matrices of the dynamic system by fitting Bode magnitudes plots using non-linear least squares. Figure 6 demonstrates the results of the SSA analysis using low-magnitude seismic records obtained in the free-field conditions and on the top floor of the instrumented structure. The natural frequencies were identified from the noisy record depicted in Figure 6(a).

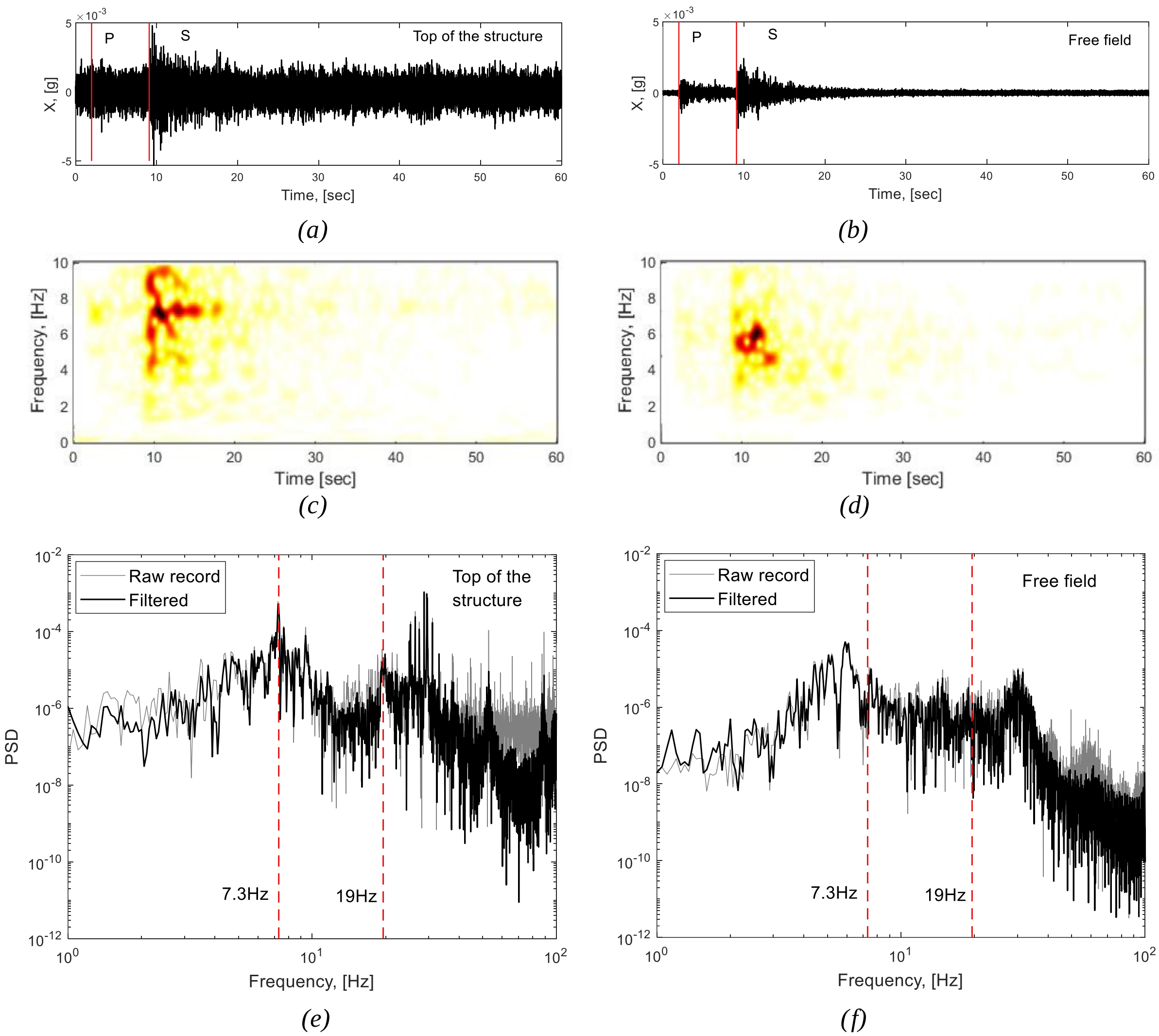

Figure 6. Acceleration records along the longitudinal direction of the structure: (a) top of the structure, (b) free-field. Corresponding Gabor wavelet amplitude spectra: (c) top of the structure, (d) free-field. Natural period identification via SSA method: (e) top of the structure, (f) free-field. Note, that eigenfrequencies are not visible in the free-field spectra (f).

SYSTEM SCALABILITY

Potential adaptation and implementation of the EEWS in other regions, potentially with other operators, requires a flexible and scalable architecture, when a number of individual stations (nodes) can be added or removed without affecting the functionality of the entire system. This feature allows the operator to optimize the total cost, which resonates with the performance-based design concept in earthquake engineering.

An important feature of this EEWS is its ability to function reliably when the number of nodes changes, a capability referred to as system scalability. Specifically, horizontal scalability is of great importance when a network has an increasing number of nodes which are separated geographically. A system architecture with horizontal scalability allows an EEWS network to be expanded even when the initial investment may be small. The initial investment in an EEWS is a function of the need to calculate the basic event parameters related to the event location, its size, and the origin time.

The client-server model of the Metro Vancouver EEWS allows for a seamless integration of additional nodes to provide enhanced geographical coverage of the instrumented region. Since one of the on-site computers acts as a server, the upper limit for the number of allowable clients is controlled by the server’s ability to handle simultaneous connections given its finite computational resources. The current implementation of the system, and the on-site industrial computers being used, can handle up to 200-300 simultaneous connections with remote clients. This can be easily increased by upgrading the hardware of the on-site computer which is assigned the role of the main server.

The network-based EEWS contains a number of important security features. It uses a layered security approach, whereby protections are implemented at the application layer, the host layer, and the network layer. In addition, short messages passing between the clients and the server use secure connection employing custom-built multiple handshaking protocol.

The EEWS at Metro Vancouver has been designed to be upgraded to handle external alert messages. Currently, a phone app is being integrated into the system, this allows the system to push notification messages to designated mobile phone users.

From Weir-Jones experience, the cost of this system is competitive with systems offering many fewer capabilities, older designs, and much higher latencies. The ease of scalability offers organizations like Metro Vancouver who operate facilities over extended geographical areas, a cost effective, integrated, and reliable EEWS.

CONCLUSIONS

This paper describes the Metro Vancouver network-based EEW system, which includes SHM components at one of its stations. The EEW algorithm represents a blend of the on-site and network-based approaches. The event characterization algorithm was validated using a KiK-net database consisting of 4,899 records of large-magnitude events. The EEW algorithm assumes a point source model, and takes into account uncertainties in the estimated event parameters.

The SHM components of the project use conventional parameters of the ground motion (i.e. response spectra and peak amplitudes of time-domain records), and inter-storey drifts to report the state of health via web-based dashboard. In addition, system identification analysis by means of the Singular Spectrum Analysis method is utilized for the off-line structural health monitoring.

The Metro Vancouver EEW and strategic response system provides operations staff early warning of a seismic event through audible alarms and digital alerts. Early warning is critical to enable staff to respond efficiently and effectively to ensure drinking water continues to be delivered throughout the region. Specifically, the purpose of the EEW and strategic response system is to: (a) alert staff and initiate automated processes such as valve operation using early warning data, (b) verify the intensity of the earthquake using strong motion data, (c) continue or reverse the automated process based on the strong motion data, and (d) evaluate the structural integrity of monitored buildings after the event. The audible alarms and digital alerts are working well and staff are trained on response procedures. Evaluation and implementation of potential automated processes are in the planning stages.

ACKNOWLEDGMENTS

The project was supported by the Greater Vancouver Water District. The authors wish to extend their appreciation to the CCEE-PCEE conference organizers.

REFERENCES

[1] Wu, Y-M., Kanamori, H., Allen, R., Hauksson, E. (2007). "Determination of earthquake early warning parameters, τ_c and P_d, for southern California". *Geoph. Journal Int*., **170**(2), 711-717. https://doi.org/10.1111/j.1365-246X.2007.03430.x

[2] Grapenthin, R., Johanson, I. A., Allen, R. (2014). "Operational real-time GPS-enhanced earthquake early warning". *J. Geophys. Res. Solid Earth*, 119, 7944–7965, doi:10.1002/2014JB011400.

[3] Kanamori, H., 2005. "Real-time seismology and earthquake damage mitigation", *Ann. Rev. Earth Planet. Sci.*, **33**, 195–214, doi:10.1146/annurev.earth.33.092203.122626.

[4] Trugman, D. T., Page, M. T., Minson, S. E., & Cochran, E. S. (2019). "Peak ground displacement saturates exactly when expected: Implications for earthquake early warning". *Journal of Geophysical Research: Solid Earth*, 124, 4642–4653. https://doi.org/10.1029/2018JB017093

[5] Chung, A.I., Henson, I., Allen, R.M. (2019). "Optimizing earthquake early warning performance: ElarmS-3". *Seism. Res. Letters*, 90(2A), 727-743

[6] Böse, M. Allen, R., Brown, H., Gua, G., Fischer, M., Hauksson, E., Heaten, T., Hellweg, M., Liukis, M., Neuhauser, D., Maechling, P., Solanki, K., Vinci, M., Henson, I., Khainovski, O., Kuyuk, S., Carpio, M., Meier, M.-A., Jordan, T. (2014). "CISN ShakeAlert: An Earthquake Early Warning Demonstration System for California". In: Wenzel, F., Zschau, J. (eds)

Early Warning for Geological Disasters. Advanced Technologies in Earth Sciences. Springer, Berlin, Heidelberg. https://doi.org/10.1007/978-3-642-12233-0
[7] Böse, M., Felizardo, C., Heaton, T.H. (2015). "Finite-fault rupture detector (FinDer): going real-time in Californian ShakeAlert Warning System". *Seism. Res. Letters*, 86(6), 1692-1704.
[8] Kodera, Y., Yamada, Y., Hirano, K., Tamaribuchi, K., Adachi, S., Hayashimoto, N., Morimoto, M., Nakamura, M., Hoshiba, M. (2018). "The Propagation of Local Undamped Motion (PLUM) Method: A Simple and Robust Seismic Wavefield Estimation Approach for Earthquake Early Warning", *Bulletin of the Seismological Society of America*, vol. 108, issue 2, pp. 983-1003.
[9] Parolai, S., Oth, A., Boxberger, T. (2017). "Performance of the GFZ Decentralized On-Site Earthquake Early Warning Software (GFZ-Sentry): Application to K-NET and KiK-Net Recordings, Japan", *Seism. Res. Letters*, **88**(6), 1480-1490.
[10] Simons, F., Dando, B., Allen, R. (2006). "Automatic detection and rapid determination of earthquake magnitude by wavelet multiscale analysis of the primary arrival". *Earth and Planetary Science Letters*, Elsevier, 250, 214-223.
[11] Minson, S.E., Baltay, A.S., Cochran, E.S., Hanks, T.C., Page, M.T., McBride, S.K., Milner, K.R., Meier, M.A. (2019). "The limits of Earthquake Early Warning Accuracy and Best Alerting Strategy". *Scientific Reports*, **9**, 2478.
[12] Zaicenco, A., Huffman, S., Weir-Jones, I. (2010). "Seismic P-wave polarization in the context of on-site early warning system". *5th Intl. Conf. on Advances in Geotech. Earthq. Eng. And Soil Dyn*., San Diego, CA, paper nr.3.12a.
[13] Zaicenco, A. and Weir-Jones, I. (2012). "Lessons Learned from Operating an On-site Earthquake Early Warning System". 15 WCEE, Lisbon, 10pp.
[14] Zaicenco, A. and Weir-Jones I. (2011). "Elastic wave polarization using EMD vs Fourier and wavelet basis". SEG Technical Program Expanded Abstracts: 4388-4392. https://doi.org/10.1190/1.3658766
[15] Weir-Jones, I. and Zaicenco, A. (2016). "Earthquake Early Warning Systems. Technology Detects, Analyses and Acts on Seismic Signals". *Innovation*, Journal of Assoc. of Prof. Eng. And Geosc. of BC, March/April, 29-32.